ISSN: 2414-1895 DOI: 10.6919/ICJE.202505_11(5).0022

Reconfigurable Topological Transport of Dual-frequency Elastic Waves in Solid Phononic Crystals

Jiangxing Xiong

School of Physics and Optoelectronic Engineering, Guangdong University of Technology, Guangzhou 510006, China

Abstract

Elastic wave topological materials have attracted much attention due to the conservation of their topological properties, which can accurately guide and control the propagation path of elastic waves. Aiming at the limitations of traditional single-frequency topological materials for multi-scenario applications, this paper proposes a dual-frequency topological phononic crystal, which realizes the synergistic effect of negative refraction at low frequencies (8.6-14.6 kHz) and zero refraction at high frequencies (32-36 kHz) through symmetry breaking modulation. The design of supercell hetero structure based on Valley Chen number inversion, combined with Berry curvature analysis, confirms that the dual-frequency topological boundary states are excited by the body-edge correspondence principle. Numerical simulations show that the elastic waves in defective or curved paths maintain very high transmission efficiency, low backscattering loss, and exhibit strong robustness; the incidence angle modulation experiments further validate the topological locking property of zero refraction. The dual-frequency topological refraction mechanism provides a new idea for multi-frequency acoustic communication, integrated acoustic chip and adaptive acoustic field regulation.

Keywords

Elastic Wave; Topological Insulator; Valley-Selective Excitation; Topological Edge States.

1. Introduction

In recent years, the deep integration of topological physics with classical wave systems has opened unprecedented avenues for manipulating acoustic and elastic waves. Inspired by quantum Hall effect (QHE), quantum spin Hall effect (QSHE), and quantum valley Hall effect (QVHE) in condensed matter physics, researchers have successfully realized robust boundary-state transmission of elastic waves through artificially designed topological phononic crystals (TPnCs). This breakthrough overcomes the defect sensitivity inherent in conventional phononic crystal bandgaps. A pivotal advancement in this field stems from precise symmetry engineering: breaking time- reversal symmetry (TRS) or spatial inversion symmetry induces topologically nontrivial band structures, thereby exciting protected edge states at material interfaces. The backscattering immunity of these states provides a theoretical foundation for designing high-robustness acoustic devices .

In elastic analogs of QSHE, He et al.proposed a honeycomb-lattice phononic crystal model, where accidental degeneracy at the Γ-point of the Brillouin zone enabled the first observation of pseudo-spin-polarized unidirectional Lamb wave propagation. Experiments demonstrated that the edge states maintained over 90% transmission efficiency even with perforations or disorder perturbations, confirming the defect immunity conferred by topological protection. Concurrently, Lu's team [8] introduced asymmetric scatterers into triangular-lattice phononic crystals, inspired by the valley degree of freedom in electronic systems, achieving "valley-polarized" boundary states. Phase-

Volume 11 Issue 5, 2025
DOI: 10.6919/ICJE.202505_11(5).0022

resolved laser vibrometry revealed that valley edge states exhibited less than 3 dB backscattering loss in Z-shaped waveguides, establishing a new paradigm for low-loss acoustic circuits. Notably, realizing QHE analogs in elastic systems demands more intricate symmetry- breaking mechanisms. Zhang et al. constructed a rotating non-inertial mass-spring honeycomb lattice, where Coriolis forces mimicked synthetic gauge fields. This approach generated helical topological edge states with group velocity linearly proportional to rotational speed ($v_g \propto \Omega_R$), enabling actively tunable acoustic topological devices without external magnetic fields.

With the maturation of TPnC theory, their application potential in functional device design has rapidly expanded. For instance, valley-topology-based acoustic mode-lockers achieve dynamic energy-splitting ratios (1:10) within 1.5-3.5 kHz , while spiral-edge-state-driven elastic circulators exhibit insertion losses below 0.5 dB in piezoelectric transducer arrays.Furthermore,energy localization at topological boundaries enhances vibration harvesting efficiency; experiments show a 300% improvement in energy conversion at 20 Hz compared to conventional structures . These advancements mark a paradigm shift from "passive bandgap engineering" to "active topological control" in acoustic metamaterials, offering innovative solutions for aerospace structural health monitoring and underwater acoustic communication .

Current challenges persist: (1) Low-frequency topological states (<1 kHz) face limitations due to conflicts between structural compactness and effective mass density; (2) The impact of multiphysics coupling (e.g., thermo-acoustic, mechano-electric interactions) on topological robustness remains poorly understood; (3) Fabrication and characterization techniques for 3D topological phononic crystals require further development.

Dual-band topology transmission and refraction will significantly improve the performance of the device and add additional bandwidth compared to single-band, thus providing great flexibility for the device.

The proposed dual-band topological refractive materials will facilitate the development of solid- state topologically integrated devices with multi-functionality, multi-band and high capability.

2. Model Construction and Band Inversion

2.1 Design of Model

The considered basic structure of the PnC plate is illustrated in Fig. 1(a), with a hexagonal honeycomb lattice (outlined by a red solid line) defining the unit cell geometry. An enlarged view of the unit cell is shown in Fig. 1(b), The green triangular prism and the three cylinders are steel, the cylinders and triangular prism connectors are aluminum, and the middle plate.

Key geometric parameters include: a lattice constant a=16 mm;circular notches of radius $r = 2\,mm$ at each hexagonal corner; a central steel triangular prism with edge length $d = 3\,mm$; and aluminum rectangular connectors(width $e_1 = 1mm$,length $e_2 = 4mm$)linking the prism to cylindrical structures (radius $R = 1.5mm$)on the upper and lower plates. The hexagonal honeycomb plate, made of epoxy resin, has a thickness $H_1 = 1mm$, while the connecting columns between plates exhibit a height $H_2 = 3mm$ .The initial rotational angle of the configuration is set to $\theta = 0°$.

The selected material parameters are as follows : the mass density of epoxy resin ρ_{Epoxy}=1180kg/m^3, Young's modulus E_{Epoxy} =3Gpa,and the Poisson's ratio v_{Epoxy} =0.3;the mass density of steel ρ_{Steel}=7850kg/m^3,Young's modulus E_{Steel}=200GPa ,and the Poisson's ratio v_{Steel} =0.3;the mass density of aluminum $\rho_{Al} = 2700kg/m^3$,Young's modulus $E_{Al} = 70\,GPa$,and the Poisson's ratio $v_{Al} = 0.33$ .This multi-material design exploits contrasts in stiffness and density to modulate elastic wave propagation, with parametric(a,r,R,d,e_1,e_2,h_1,h_2) control over geometric variables enabling precise engineering of band gap properties for tailored dynamic responses.

In the Solid Mechanics module of COMSOL Multiphysics, the energy band structure and displacement field distribution of in-plane polarized bulk elastic waves in a phononic crystal system are investigated using numerical analysis. In order to resolve the dispersion relations in the bulk (edge) energy bands, Floquet periodic boundary conditions are applied to individual crystal cells (or supercell configurations). This computational approach involves scanning the wavevector within the first Brillouin zone as in Fig.1(c). Under condition C_{3v}, the phononic crystal lattice exhibits spatial symmetry, leading to a simple merging of the energy bands at the high symmetry point, K.

As a result, as shown in Fig. 1(e), two Dirac cones at both low and high frequencies appear in the energy band structure within the first Brillouin zone, corresponding to the frequencies at f = 10.82 kHz and f = 32.44 kHz, reflecting the unique topological properties of the system. We denote the phonon crystal structure at a rotation angle of θ = 0° as Cell A.

To explore topological phase transitions. When the rotation angle θ is greater than 0° or less than 0°, the spatial symmetry of the cell changes. This change leads to the splitting of Dirac points and the formation of a band gap (as shown in the shaded region in Fig. 1(e). Points split from the Dirac cone can be labeled as p_1^+ (p_2^+) or q_1^- (q_2^-) states, respectively. The symbols "-" or "+" indicate the clockwise or counterclockwise direction of the elastic wave mechanical energy flow map.

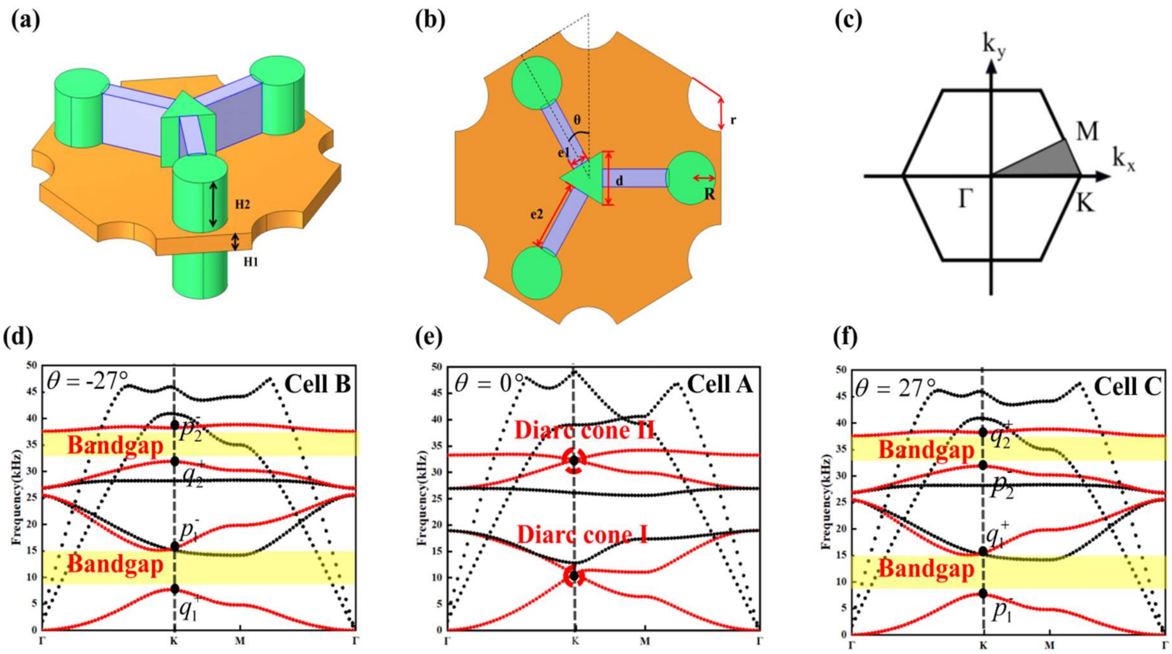

Fig. 1 Schematic diagrams of the unit cell with C_3 rotational symmetry and Band structure of phononic crystals(a) Three-dimensional perspective view of the phononic crystal unit cell.(b) Planar projection view of the unit cell, where θ denotes the orientation angle of the aluminum rectangular prism relative to the positive y-axis.(c) Schematic of the first irreducible Brillouin zone (gray hexagonal region) and its boundary path (Γ–K–M–Γ), defining the wavevector (k) trajectory for band calculations.(e) Band structure of the phononic crystal with the scattering unit (denoted as Cell A) at a rotation angle of θ = 0°. Two Dirac points emerge at the high-symmetry K point of the Brillouin zone.(d) Band structure for Cell B (scattering unit rotated by θ=–27°)showing a bandgap (highlighted in yellow)induced by symmetry breaking. (f) Band structure for Cell C (scattering unit rotated by θ = +27°), exhibiting a similar bandgap topology but with reversed valley-polarized states compared to (d)

In order to quantitatively study the topological phase at the bandgap boundary, we introduce the nonzero valley Chern number and k-p regimes methods. First, from the k-p regimes method one can derive the effective Hamiltonian quantity in the neighborhood of the Dirac point,which can be expressed as:

ISSN: 2414-1895 DOI: 10.6919/ICJE.202505_11(5).0022

$$H = v_D(\delta k_x \sigma_x + \delta k_y \sigma_y) + \Delta_g \sigma_z \tag{1}$$

In Equation. (1) v_D is the effective group velocity near the Dirac point when the scatterer is not rotating, δk_x and δk_y denote the momentum space wave vectors in the offset near the K point, and δ_i is the Pauli matrix corresponding to the chiral pseudospin. When the scatterer turn angle of $\theta \neq 0°$ is satisfied, the frequency band gap between the upper and lower energy valleys can be expressed as $2\Delta = f_+ - f_-$, where the positive and negative signs of the subscripts correspond to the scatterer angle $\theta \neq 0°$, respectively. scatterer turning angles $\theta > 0°$, $\theta < 0°$, corresponding to the gray and yellow regions, and the green and fan regions in Fig. 2(a).

When the angle $\theta = 0°$, the p-states and q-states undergo a simple merger, resulting in 2 Dirac points, which are located at the frequencies of f =10.82 kHz and f = 32.44 kHz; when $\theta = 27°$ or $\theta = -27°$, the simple merger of Dirac points is turned on, and the Dirac points are located at the frequencies of f =10.82 kHz and f =32.44 kHz. The simple merger at the point is opened, at this time two valley states with opposite spin directions are obtained on the p and q states in the Fig. 1(d) and Fig. 1(f) energy bands, and a forbidden band is created between these two valley states.

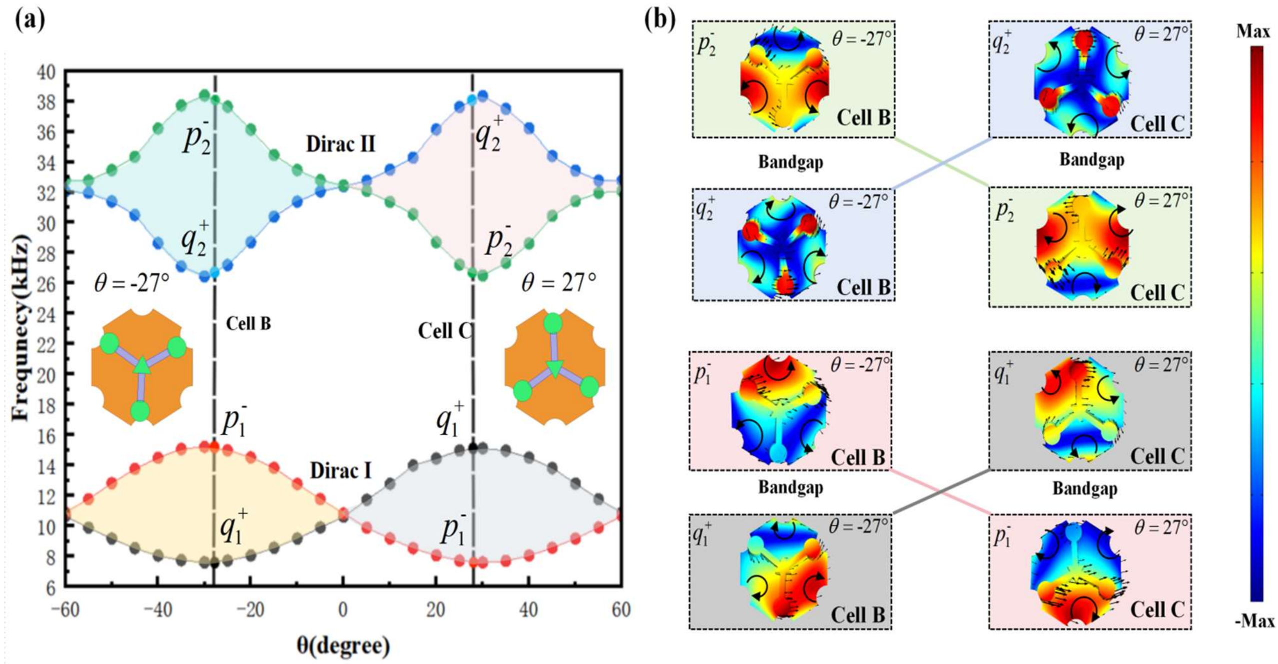

Fig. 2 Energy band inversion and conversion results for different valley states (a) Frequency variations of the p- and q-states at different angles of rotation, where q_1^+ p_1^-, q_2^+ p_2^- for Cell B are for the rotation angle θ =-27°, and where q_1^- p_1^+, q_2^- p_2^+ for Cell C are for the selected angle θ =27° (b) Phase diagrams of the intrinsic field pressure field at the valley state at the K point. The corresponding rotation angles are θ = -27° (left column plots) and θ = 27° (right column plots).It exhibits opposite vortex chirality at both high and low frequencies, reflecting the resultant response of the topological phase transition

In order to deeply characterize the topological properties of the system, this study constructs a framework for geometrical phase analysis in momentum space based on the Berry phase theory. In

ISSN: 2414-1895 DOI: 10.6919/ICJE.202505_11(5).0022

the crystal momentum (k) space, the Berry contact $A_n(k)$ and Berry curvature $\Omega_n(k)$ can be defined as respectively:

$$A_n(k) = i\langle \mathrm{u}_{\mathrm{nk}} \,|\, \nabla_k \,|\, u_{nk} \rangle \tag{2}$$

$$\Omega_n(\vec{k}) = \nabla_k \times \langle \mathrm{u}_{\mathrm{nk}} \,|\, i\nabla_k \,|\, u_{nk} \rangle = \frac{\Delta_{\mathrm{g}} / v_D}{2(\delta k^2 + \Delta_{\mathrm{g}}^2 / v_D^2)^{-3/2}} \tag{3}$$

where $u_n(k)$ is the periodic component of the nth Bloch wave function. By integrating the Berry curvature near the K-valley in the Brillouin zone, the valley Chen's number, a topological invariant characterizing the valley polarization properties, is obtained:

$$C = \frac{1}{2\pi} \int_{HBZ} \Omega(\vec{k}) d\vec{k} = \frac{1}{2}\mathrm{sgn}(\Delta_g) \tag{4}$$

The theoretical analysis of Equation. (4) shows that the sign of the valley Chen's number is determined by the geometric phase difference Δ_g.When the scatterer undergoes clockwise rotation,the Chen's numbers corresponding to the K and K' valleys are $C_{q^-} = 1/2$ and $C_{q^+} = -1/2$ respectively;when rotating counterclockwise($\theta < 0°$),they show the opposite sign distributions, That is, $C_{q^-} = -1/2$ and $C_{q^+} = 1/2$. Since the system maintains time-reversal symmetry, the total Chen's numbers $C = C_{q^-} + C_{q^+}$ remains strictly zero-valued in character, and this symmetry constraint drives the system to produce acoustic valley Hall phase separation.

Numerical calculations show that the Berry curvature exhibits a singularity abrupt change in momentum space when $\theta = 0°$, and this critical point corresponds to the topological phase transition threshold for symmetry breaking of the system $C_{3\mathrm{v}}$.When $\theta \neq 0°$, the spatial symmetry breaking induces the splitting of the Dirac cone simple merger state and the formation of an energy band structure with valley polarization characteristics. This is manifested as follows: for $\theta > 0°$, the K valley splits into p_1^+ and p_2^+ states (corresponding to counterclockwise pseudospin flow), and the K' valley splits into q_1^- and q_2^- states (corresponding to clockwise pseudospin flow); for $\theta < 0°$, the direction of the polarization is reversed, and the sign of the valley Chen's number is reversed from that of the former.

This mechanism of Valley Chen's number modulation based on the rotational transformation of the scatterer provides a theoretical basis for the construction of heterogeneous topological interfaces. When two Valley Hall phase insulators with the same bandgap structure but opposite Valley Chen's numbers ($C_{q^+} = \pm 1/2$, $C_{q^+} = \mp 1/2$) form an interface, topologically protected edge states will be generated at the interface according to the body-edge correspondence principle. Theoretical calculations confirm that the difference in the number of valley chanes at the interface of such heterostructures is $\Delta C_{\mathrm{q}} = \pm 1$,and this nonzero topological invariant directly leads to the localized character of the boundary states in the bandgap range.In this study, the intrinsic correlation mechanism between the acoustic valley Hall effect and the geometrical phase modulation is revealed by systematically analyzing the Berry curvature distribution law at different rotation angles.

2.2 Topological Edge State

In topological insulator material systems, the generation of boundary states originates from the quantum state properties triggered by the surface plasmon resonance effect, and such edge states with topologically protected features construct a barrier against external interference for acoustic topological insulators (ATIs).It is shown that the energy localization phenomenon generated by the coupling of the phonon vibrational modes with the plasma resonance effect in ATIs is the core mechanism to realize the surface fluctuation confinement.In order to deeply investigate the superconducting properties and acoustic transport law of ATIs, this study adopts the design strategy of coupling topologically mediocre and non-mediocre structures to construct a composite supercell system.

Based on the finite element numerical calculation method, the energy band characteristics of the supercell cells can be resolved by applying periodic boundary conditions along the lattice vector direction.By regulating the spatial arrangement of B-type (θ = -27°) and C-type (θ = 27°) cells, the dynamic reconfiguration of the edge transport paths of different configurations can be realized. As shown in Fig. 3(a), the designed supercell consists of 10 groups of B-type cells and 10 groups of C-type cells arranged alternately along the y-axis, in which the structural parameters and material properties of each cell are consistent with the above.

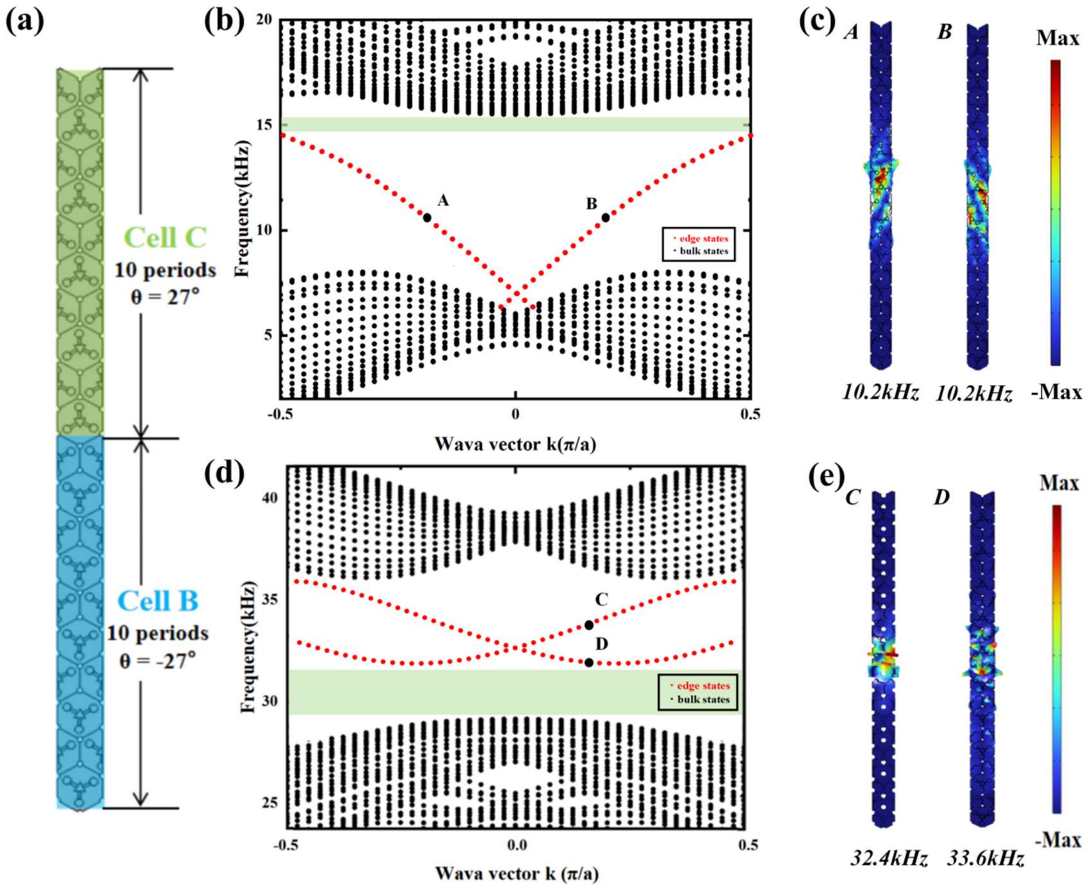

Fig. 3 Valley topological acoustic waveguide with acoustic waves mainly confined in the domain walls(a) The supercell structure consists of 10 Cell C-type (θ = 27°) structures and 10 Cell B-type (θ = -27°) structures (b) and (d) are the supercell dispersion diagrams of the in-plane polarized elastic wave modes, with the red lines denoting the edge states.

According to the body-edge correspondence principle, boundary states are induced at the interfaces of heterogeneous structures due to abrupt changes in the physical properties and geometrical configurations of the materials.The mechanism of such interfacial states can be attributed to 1) the discontinuity of the bandgap structure of the heterogeneous unit leading to the overlapping of energy bands, and 2) the redistribution of the density of electronic states induced by the distortion of the atomic arrangement in the interfacial region. It is noteworthy that the boundary-state energy levels are strictly distributed within the bulk bandgap, and their spatial locality originates from the coherent superposition effect of quantum states at the interface.This bandgap-selective boundary state provides theoretical support for the design of novel acoustic waveguide devices.

In the energy band analysis of the supercell structure using the finite element numerical method, the dispersion characteristic maps shown in Fig.3(b) and Fig.3(d) are successfully obtained by applying Fourier boundary constraints on the upper and lower surfaces of the supercell model.The black background region in the maps corresponds to the bulk wave propagation properties, and the red eigenlines characterize the dispersion relations of the interface states.It is noteworthy that the CB composite structure, which consists of Cell C and Cell B units, exhibits significant bandgap characteristics in both the frequency domains of 8.6kHz-14.6 kHz (fundamental frequency band) and 32-36 kHz (high frequency band).

It is particularly noteworthy that the effective frequency range of the interface states does not completely occupy the entire body bandgap region, but forms a unique interface bandgap structure inside the two bandgaps.In the fundamental frequency bandgap range, the interfacial bandgap is located at the upper edge of the energy band of the interfacial state (corresponding to the light-green labeled region),while in the high-frequency bandgap,it shows the lower edge distribution characteristics.This interface state distribution with bandgap modulation provides an important physical basis for the system to generate topological angular states.

Thanks to the protected boundary states at the interface between topologically non-trivial and conventional structures, elastic waves can be transmitted losslessly at interfaces of arbitrary shapes, including straight or curved.Numerical calculations show that the fluctuating energy exhibits an exponential decay when it tries to diffuse to both sides of the structure, thus ensuring that the fluctuating energy is strictly confined to the interface region.The metamaterial system constructed in this study has a wide range of non-trivial bandgap properties, and this special design not only endows the system with strong robustness against structural defects, but also demonstrates significant advantages at the level of engineering measurements and practical applications.Simula- tion experiments confirm that this topology has excellent immunity to acoustic wave transmission disturbances, which is of great value in the field of acoustic modulation and vibration control.

And Fig. 3(c) depicts the displacement field distribution at points A and B corresponding to the bilateral bandgap in the low frequency band. It can be seen that the maximum displacement amplitude is mainly concentrated in Cell C and Cell B types directly to the interface, and when moving away from the interface, the displacement amplitude decays rapidly until it disappears. Similarly, in Fig. 3(e), the shift field distributions at points C and D in the high-frequency band are also concentrated between the interfaces, which indicates that these topological boundary states can be well localized in the interface states.

Boundary states that can localize waves at the interface of the two metastable cells exist in both the low and high frequency body bandgaps, and such modes can achieve directional guidance of acoustic waves, providing a means to finely manipulate the directional transmission of acoustic waves.

3. Valley Edge State and Robust Transport

TESs have remarkable properties, especially their robustness in boundary transport. These topology-protected boundary states can traverse any boundary, straight or curved, exhibiting exceptional transmission properties with minimal reproduction and loss.

Volume 11 Issue 5, 2025
DOI: 10.6919/ICJE.202505_11(5).0022

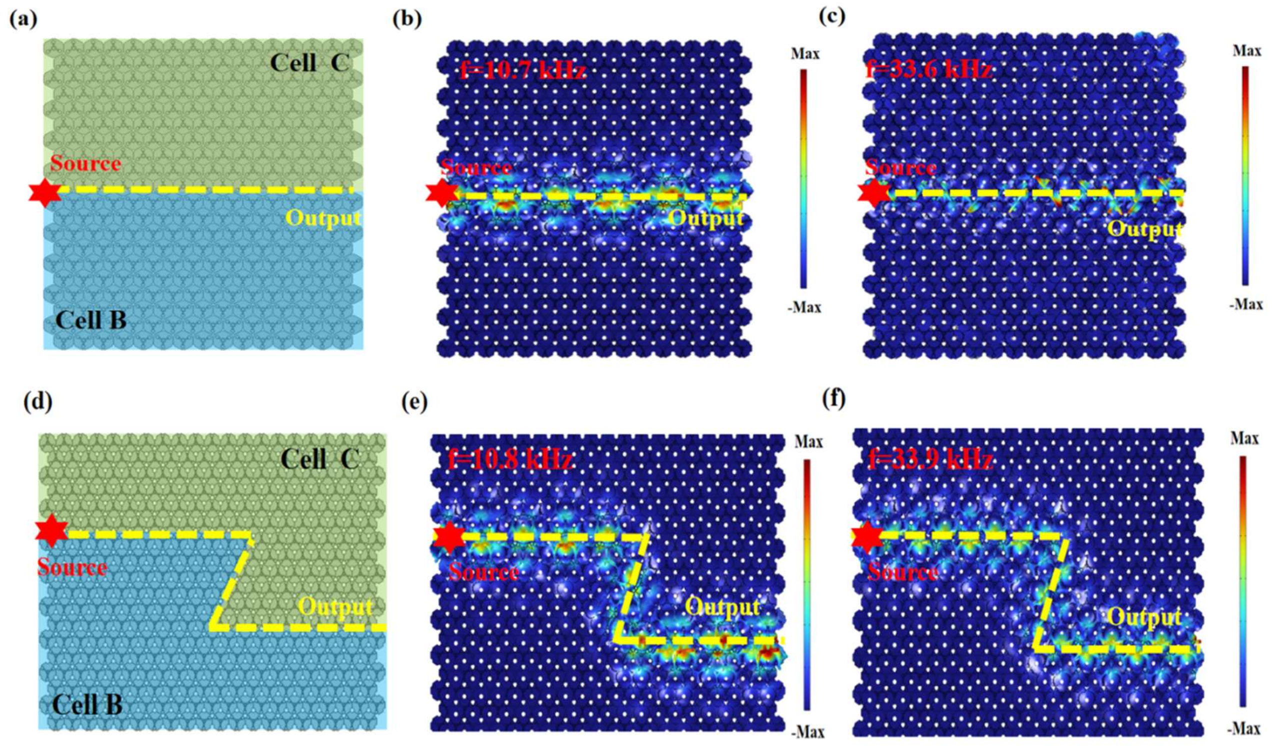

Fig. 4 Transmission effects in energy valley-locked linear and zigzag boundary structures (a) and Fig. (d) represent Cell C-type and Cell B-type through linear and zigzag splicing, consisting of topological and non-topological states, with the excitation point source at the six-pointed star (b) and (d) represent the displacement fields of linear-type low-frequency and high-frequency at the excitation frequencies of f = 10.7 kHz and f = 33.6 kHz, respectively, with simultaneous topological transmission phenomena (b) and (d) represent the displacement field of linear-type low-frequency and high-frequency at the excitation frequency of f = 10.7 kHz and f = 33.6 kHz, respectively, with simultaneous(e)and(f) epresent the displacement fields of zigzag low-frequency and high-frequency at the excitation frequencies f = 10.8 kHz and f = 33.9 kHz, respectively, while the topological transmission phenomenon occurs.

Thus, topologically protected boundary states can stably transmit information in a variety of situations, even if the boundaries are curved or broken.Here, we try to study the wave propagation behavior, i.e., trapping and waveguiding at different frequencies and paths.

As shown in Fig. 4(a) and Fig. 4(d), the blue domains denote Cell B cells and the green domains denote Cell C cells. Using this design, a straight wave propagation path and a Zigzag propagation path are formed, and the linear type is a supercell consisting of 20×16 protocells, in as in Fig. 4(a), we can see the hexagonal star out as the excitation point source, and then transmit at both high and low frequencies, Fig. 4(b) and Fig. 4(c) shows the case when the excitation point source is f = 10.7 kHz, and f = 33.6 kHz. displacement field maps of the supercell. Compared to Fig. 4(c)and Fig. 4(e) this case enlarges the topological valley locking layer. Similarly we performed a Zigzag propagation path in the supercell consisting of 20×20 protocells, excited with different frequencies at f = 10.8 kHz and f = 33.9 kHz high and low frequencies, and the displacement field maps in the supercells similarly found that the waves propagate along the Zigzag boundaries well being localized.

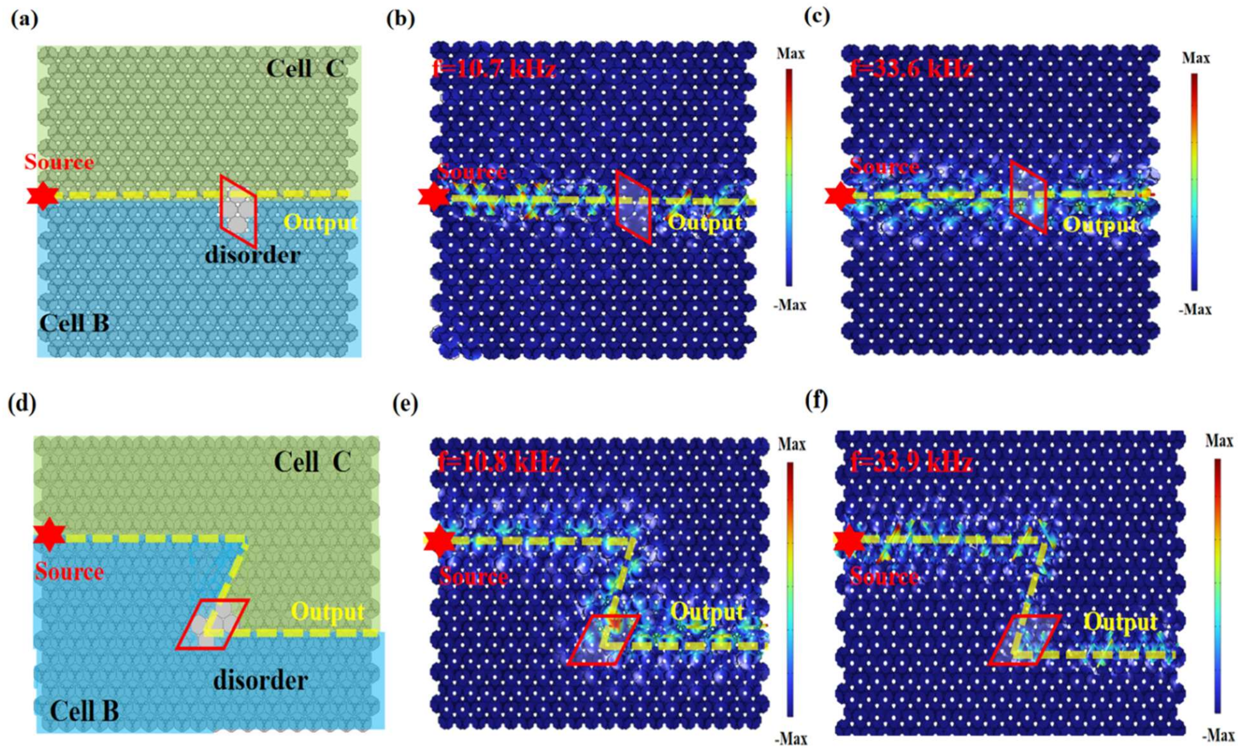

Fig. 5 Validation of robustness of Noh valley-locked linear and zigzag topological transmission Fig. (a) (d) represent represent Cell C-type and Cell B-type via linear and zigzag splicing respectively, consisting of topological and non-topological states, with the excitation point source at the six-pointed star in (b) (c) shows the displacement field of a linear supercell with defects at frequencies f = 10.7 kHz and f = 33.6 kHz excitation point source in (e) (f) is the displacement field of the zigzag supercell with defects at frequency f = 10.8 kHz and f = 33.9 kHz excitation point source

And one of the most important features of topological boundary states is that the backscattering due to their defects can be neglected at phononic crystal interfaces or when defects exist at the interfaces.

To further demonstrate the defect immunity of topologically protected wave transport. We set a defect in the path of linear and Zigzag topological transport and follow the same point excitation source with the same frequency wave to excite, here also take Cell B-Cell C splicing, as shown in Fig. 6(a)and Fig. 6(d), and its eigenfields are shown in Fig. 6(b)-(c)and Fig. 6(e)-(f), and it is found that the wave can still continue to propagate bypassing the defect, and it does not cause strong scattering. The profound path design in controlling the defect-immunized elastic wave transmission can be easily achieved without backscattered waves and realizing high quality concentration of the input energy.

4. Conclusion

In this study, a new mechanism for acoustic topology modulation based on controllable rotating scatterers is proposed.

Efficient manipulation of the valley Hall topological phase transition is realized by rotational transformation of the scatterer at a specific angle. The C3v symmetric layered phononic crystal system constructed in the study exhibits multiple linear Dirac cones at the K-point of the Brillouin zone, which provides a physical basis for multi-band acoustic wave modulation. Scatterer angle modulation can break the symmetry of the system and induce the splitting of the Dirac point simplex state, which leads to the formation of a topologically non-trivial bandgap with valley Hall effect. This dynamic modulation can realize the flexible switching of valley pseudo-spin states without reconfiguring the lattice substrate.

Based on the body-edge correspondence principle, acoustic topological interface states with dual-frequency bandgap characteristics are successfully constructed in this study. Experimental and simulation verifications show that by designing heterogeneous supercells with Cell B (θ=-27°) and Cell C (θ=27°) arranged alternately, topologically protected edge-transport modes can be excited within the fundamental (8.6kHz-14.6 kHz) and high-frequency (32-36 kHz) bandgaps, respectively. Typical application examples demonstrate the innovative design of a dual-channel beam splitter with a single waveguide isolator, the core mechanism of which originates from the directional confinement effect of the interface states on the acoustic energy.

The regulation method breaks through the design limitations of traditional acoustic devices with three innovative features: (i) univariate control of angular rotation to realize complex topological phase transitions; (ii) programmable design of multi-frequency acoustic boundary states; and (iii) topological protection mechanism to give the device anti-jamming characteristics. This topological acoustic control platform opens up a new path for a new generation of intelligent acoustic systems, and shows important application value in the fields of acoustic sensing, quantum acoustic chips and multi-channel communication, especially in the robust acoustic signal processing in complex acoustic field environments, with unique advantages.

References

[1] P. Bampoulis, C. Castenmiller, D.J. Klaassen, J. van Mil, Y.C. Liu, C.C. Liu, Y. G. Yao, M. Ezawa, A.N. Rudenko H J W Zandvliet, Quantum spin hall states and topological phase transition in germanene, Phys. Rev. Lett. 19 (2023) 196401.

[2] Hasan M Z, Kane C L 2010 Rev. Mod. Phys. 82 3045

[3] Xie B Y, Su G X, Wang H F, Su H, Shen X P, Zhan P, Lu M H, Wang Z L, Chen Y F 2019 Phys. Rev. Lett. 122 233903.

[4] C.F. Li, R. Wang, S. Zhang, Y.Y. Qin, Z. Ying, B.Y. Wei, Z. Dai, F.Y. Guo, W. Chen, R. Zhang, B.G. Wang, X.F. Wang F Q Song, Observation of giant non-reciprocal charge transport from quantum Hall states in a topological insulator, Nat. Mater. (2024).

[5] S. Yves, R. Fleury, F. Lemoult, M. Fink G Lerosey, Topological acoustic polaritons: robust sound manipulation at the subwavelength scale, New J. Phys. (2017) 075003.

[6] P.P. Zheng, C.I. Timms M H Kolodrubetz, Anomalous Floquet-Anderson insulator with quasiperiodic temporal noise, Phys. Rev. B 9 (2023) 094207.

[7] L.P. Ye, C.Y. Qiu, J.Y. Lu, X.H. Wen, Y.Y. Shen, M.Z. Ke, F. Zhang Z Y Liu, Observation of acoustic valley vortex states and valley-chirality locked beam splitting, Phys. Rev. B 17 (2017) 174106.

[8] Z.W. Zhang, Y. Tian, Y.H. Wang, S.X. Gao, Y. Cheng, X.J. Liu J Christensen, Directional acoustic antennas based on valley-hall topological insulators, Adv. Mater. 36 (2018) 1803229.

[9] C.X. Deng, Y.Q. Yang, J. Li, X. Zhang, Y.J. Yu, Q. Lu H Yang, Asymmetric transport in sonic valley Hall insulators, Phys. Rev. Appl. 3 (2024) 034048.

[10] M. Gulzari, Q. Zhang, E. King, L.H. Tong S K Lai, Valley edge states with opposite chirality in temperature dependent acoustic media, J. Phys. D-Appl. Phys. 34 (2024) 345303.

[11] J.F. Han, F. Liang, Y.L. Zhao, J.L. Liu, S.C. Wang, X.R. Wang, D.S. Zhao B Z Wang, Valley kink states and valley-polarized chiral edge states in substrate-integrated topological

[12] Zhao Y, Zhou X, Huang G. Non-reciprocal Rayleigh waves in elastic gyroscopic medium. J Mech Phys Solids 2020;143:104065.

[13] Yu S-Y, He C, Wang Z, Liu F-K, Sun X-C, Li Z, et al. Elastic pseudospin transport for integratable topological phononic circuits. Nat Commun 2018;9:3072.

[14] Mousavi SH, Khanikaev AB, Wang Z. Topologically protected elastic waves in phononic metamaterials. Nat Commun 2015;6:8682.

[15] Chen Y, Liu X, Hu G. Topological phase transition in mechanical honeycomb lattice. J Mech Phys Solids 2019;122:54–68.

[16] Wu Q, Chen H, Li X, Huang G. In-plane second-order topologically protected states in elastic kagome lattices. Phys Rev Appl 2020;14:014084.

[17] Pal RK, Ruzzene M. Edge waves in plates with resonators: an elastic analogue of the quantum valley Hall effect. New J Phys 2017;19:025001.

[18] Fleury R, Khanikaev AB, Alù A. Floquet topological insulators for sound. Nat Commun 2016;7:11744.

[19] Vila J, Pal RK, Ruzzene M. Observation of topological valley modes in an elastic hexagonal lattice. Phys Rev B 2017;96:134307.

[20] Li G-H, Ma T-X, Wang Y-Z, Wang Y-S. Active control Z.W. Zhang, Y. Tian, Y. Cheng, Q. Wei, X.J. Liu J Christensen, Topological acoustic delay line, Phys. Rev. Appl. 3 (2018) 034032.

[21] J.Q. Wang, Z.D. Zhang, S.Y. Yu, H. Ge, K.F. Liu, T. Wu, X.C. Sun, L. Liu, H.Y. Chen, C. He, M.H. Lu Y F Chen, Extended topological valley-locked surface acoustic waves, Nat. Commun. 1 (2022) 1324.

[22] M.D. Wang, W.Y. Zhou, L.Y. Bi, C.Y. Qiu, M.Z. Ke Z Y Liu, Valley-locked waveguide transport in acoustic heterostructures, Nat. Commun. (2020) 1.

[23] K.K. Chen, X.J. Dong, P.L. Gao, J.Y. Zhang, Y.T. Sun, G.W. Tu Z K Peng, Multifunctional applications of topological valley-locked elastic waves, Int. J. Mech. Sci. (2023) 108589.

[24] W.T. Yuan, Y.X. Zhang, Y.D. Pan, Y. Huang, J.F. Zhao, F. Yang Z Zhong, Topological rainbow trapping, concentration and guiding in graded elastic valley phononic crystal plate, Eng. Struct. (2024) 117596.

[25] M.T. Tan, X.W. Sun, Y.H. Liu, X.L. Gao, L.W. Hu T Song, Selective topological valley transport of elastic waves in a Bragg-type phononic crystal plate, J. Appl. Phys. 24 (2024) 243107.

[26] B.B. Wang, D. Jia, Y. Ge, S.Q. Yuan H X Sun, Acoustic suppressed topological refraction in valley sonic crystals, New J. Phys. 11 (2022) 113033.

[27] H.B. Huang, S.Y. Huo J J Chen, Subwavelength elastic topological negative refraction in ternary locally resonant phononic crystals, Int. J. Mech. Sci. (2021) 106391.

[28] D. Jia, Y. Ge, H.R. Xue, S.Q. Yuan, H.X. Sun, Y.H. Yang, X.J. Liu B L Zhang, Topological refraction in dual-band valley sonic crystals, Phys. Rev. B 14 (2021) 144309.

[29] Q.F. Wang, X.X. Li, P. Zhang, Y. Qin, G.C. He, M.X. Li C X Cai, Double-banded topology valley transport, Phys. Lett. A (2023) 129002.

[30] J.Y. Lu, C.Y. Qiu, L.P. Ye, X.Y. Fan, M.Z. Ke, F. Zhang Z Y Liu, Observation of topological valley transport of sound in sonic crystals, Nat. Phys. 4 (2017) 369.

[31] M. Yan, J.Y. Lu, F. Li, W.Y. Deng, X.Q. Huang, J.H. Ma Z Y Liu, On-chip valley topological materials for elastic wave manipulation, Nat. Mater. 11 (2018) 993.

[32] J. Mei, Y. Wu, C.T. Chan Z Q Zhang, First-principles study of Dirac and Dirac-like cones in phononic and photonic crystals, Phys. Rev. B 3 (2012) 035141.